Scattering by a Lossy Dielectric Cylinder in a Rectangular Waveguide

ROLAND GESCHE, MEMBER, IEEE, AND NORBERT LÖCHEL

Abstract—**Electromagnetic fields in a rectangular waveguide containing a lossy dielectric cylinder are investigated by means of the orthogonal expansion method. The calculated results are proved by measurement. Resonance effects become visible by frequency responses of the scattering parameters and understandable by patterns of magnetic fields and Poynting vectors. The lowest resonance is nonsymmetric and can be used to realize tunable bandstop filters with a relative 3-dB bandwidth of about 0.04 and an attenuation of more than 40 dB.**

I. Introduction

CYLINDRICAL OBSTACLES in a rectangular waveguide are used in many microwave devices. Since high-permittivity dielectric materials with low losses and eligible temperature coefficients are available, filter structures become important applications of dielectric obstacles in waveguide structures.

This paper investigates the structure of the dielectric cylinder in a rectangular waveguide shown in Fig. 1 considering the following restrictions:

- Incident fields are of the TE_{m0} mode.
- The axis of the cylindrical obstacle is parallel to the electric field vector.
- The dielectric is assumed to be isotropic, homogeneous, and linear, it may have losses.
- The obstacle extends over the entire waveguide height and can be displaced from the waveguide center.
- The waveguide walls are ideal conductors.

Considerable effort has been made by many authors to investigate the physical effects in such structures. To improve the approximations given in [1]–[3], Nielsen applied the point-matching method [4], [5], which has been modified in [6] and [7]. Multiple current sources are used to describe scattering by dielectric and ferrimagnetic cylinders [8]–[12], and some authors have investigated similar problems [13]–[16]. Lauterjung [17] applied the orthogonal expansion method, which was modified to analyze the present structure [18]–[20].

The orthogonal expansion method yields very reliable and accurate values for the scattering parameters. Furthermore, fields and Poynting vectors can be investigated. This allows a physical interpretation of the occurring resonance effects, which has not been done in those previous papers using other methods [1]–[16]. With the method described here, a better understanding of filters using dielectric rods becomes possible. These advantages justify the analytical and numerical effort of the orthogonal expansion method.

Manuscript received April 21, 1987; revised August 3, 1987.

R. Gesche was with the Department of Theoretical Electrical Engineering, Technical University of Darmstadt. He is now with Leybold AG, 8755 Alzenau, West Germany.

N. Löchel is with the Transmission Systems Division, Siemens AG, 8000 München, West Germany.

IEEE Log Number 8717581.

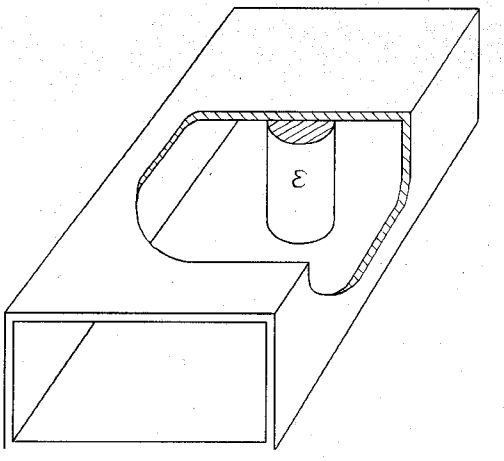

Fig. 1. Rectangular waveguide with dielectric cylinder.

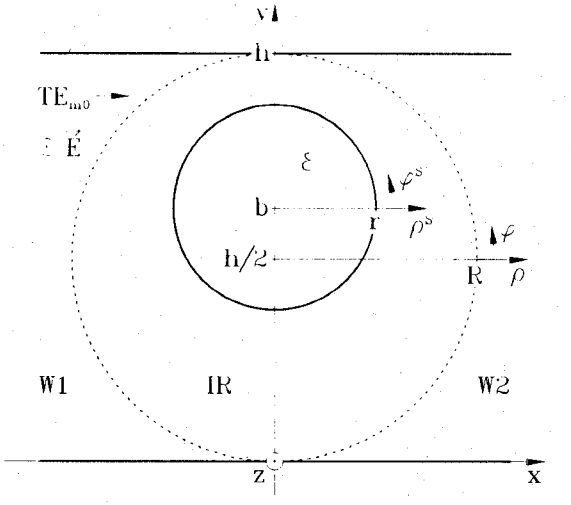

Fig. 2. Geometry of the investigated structure.

II. Mathematical Formulation

Fig. 2 shows the geometry of the investigated structure and the location of the coordinate systems used. The structure consists of two waveguide regions (W1, W2) and

0018-9480/88/0100-0137$01.00 ©1988 IEEE

a cylindrical interaction region IR [21]–[23]. The fields of the incident TE_{m0} mode and all scattered fields are independent of the z coordinate. Therefore, it is sufficient to consider the scattering problem with the three field components E_z, H_φ, and H_ρ. These fields can be derived from a vector potential [24]:

$$\vec{A} = A_z \vec{e}_z e^{j\omega t} \qquad \vec{H} = \nabla \times \vec{A} \qquad \vec{E} = \frac{1}{j\omega \epsilon_{(0)}} (\nabla \times \vec{H}). \quad (1)$$

The dielectric losses are considered by a complex permittivity:

$$\epsilon_{(0)} = \begin{cases} \epsilon = \epsilon_0 \epsilon_r (1 - j \tan\delta) & \text{inside the dielectric cylinder} \\ \epsilon_0 & \text{outside the dielecric cylinder.} \end{cases} \quad (2)$$

A. Fields in the Interaction Region

First, the fields are regarded in the coordinates of the dielectric cylinder ρ^S, φ^S, z. Taking the revolution condition into account, the wave equation solution reads

$\rho^S < r$:

$$A_z = a_0^t J_0(k_t \rho^S) \frac{1}{\sqrt{2\pi}} + \sum_{n=1}^{\infty} \left\{ a_n^{ts} J_n(k_t \rho^S) \frac{\sin(n\varphi^S)}{\sqrt{\pi}} + a_n^{tc} J_n(k_t \rho^S) \frac{\cos(n\varphi^S)}{\sqrt{\pi}} \right\} \quad (3)$$

$\rho^S \geq r$:

$$A_z = a_0^J J_0(k\rho^S) \frac{1}{\sqrt{2\pi}} + a_0^Y Y_0(k\rho^S) \frac{1}{\sqrt{2\pi}} + \sum_{n=1}^{\infty} \left\{ a_n^{Js} J_n(k\rho^S) \frac{\sin(n\varphi^S)}{\sqrt{\pi}} + a_n^{Jc} J_n(k\rho^S) \frac{\cos(n\varphi^S)}{\sqrt{\pi}} + a_n^{Ys} Y_n(k\rho^S) \frac{\sin(n\varphi^S)}{\sqrt{\pi}} + a_n^{Yc} Y_n(k\rho^S) \frac{\cos(n\varphi^S)}{\sqrt{\pi}} \right\} \quad (4)$$

$$k = \omega\sqrt{\epsilon_0 \mu_0} \qquad k_t = \omega\sqrt{\epsilon \mu_0}. \quad (5)$$

The amplitudes of (3) and (4) are arranged in vectors:

$$\vec{a}^t = \begin{bmatrix} a_0^t \\ a_1^{ts} \\ a_2^{ts} \\ \vdots \\ a_1^{tc} \\ a_2^{tc} \\ \vdots \end{bmatrix} \qquad \vec{a}^J = \begin{bmatrix} a_0^J \\ a_1^{Js} \\ a_2^{Js} \\ \vdots \\ a_1^{Jc} \\ a_2^{Jc} \\ \vdots \end{bmatrix} \qquad \vec{a}^Y = \begin{bmatrix} a_0^Y \\ a_1^{Ys} \\ a_2^{Ys} \\ \vdots \\ a_1^{Yc} \\ a_2^{Yc} \\ \vdots \end{bmatrix}. \quad (6)$$

The continuity conditions on the cylinder surface $\rho^S = r$ yield

$$\vec{a}^Y = \boldsymbol{\xi} \cdot \vec{a}^J \qquad \vec{a}^t = \boldsymbol{\eta} \cdot \vec{a}^J \quad (7)$$

$$\boldsymbol{\xi} = \begin{bmatrix} \xi_0 & & & & & & \\ & \xi_1 & & & & 0 & \\ & & \xi_2 & & & & \\ & & & \ddots & & & \\ & & & & \xi_1 & & \\ & 0 & & & & \xi_2 & \\ & & & & & & \ddots \end{bmatrix}$$

$$\boldsymbol{\eta} = \begin{bmatrix} \eta_0 & & & & & & \\ & \eta_1 & & & & 0 & \\ & & \eta_2 & & & & \\ & & & \ddots & & & \\ & & & & \eta_1 & & \\ & 0 & & & & \eta_2 & \\ & & & & & & \ddots \end{bmatrix} \quad (8)$$

$$\xi_n = \frac{J_n'(kr) J_n(k_t r) - \sqrt{\frac{\epsilon}{\epsilon_0}} J_n(kr) J_n'(k_t r)}{\sqrt{\frac{\epsilon}{\epsilon_0}} Y_n(kr) J_n'(k_t r) - Y_n'(kr) J_n(k_t r)}, \qquad n = 0,1,2,\cdots \quad (9)$$

$$\eta_n = \frac{J_n(kr) + \zeta_n Y_n(kr)}{J_n(k_t r)}, \qquad n = 0,1,2,\cdots \quad (10)$$

where the prime symbol denotes the derivative with respect to argument.

The fields in the coordinate system of the dielectric cylinder (eqs. (3) and (4)) will now be shifted to the coordinate system of the interaction region ρ, φ, z using the transformation given in [25]. It is sufficient to formulate the wave equation solution in the interaction region outside the region of the dielectric cylinder:

$\rho \geq r + \left| b - \frac{h}{2} \right|$:

$$A_z = b_0^J J_0(k\rho) \frac{1}{\sqrt{2\pi}} + b_0^Y Y_0(k\rho) \frac{1}{\sqrt{2\pi}} + \sum_{p=1}^{\infty} \left\{ b_p^{Js} J_p(k\rho) \frac{\sin(p\varphi)}{\sqrt{\pi}} + b_p^{Jc} J_p(k\rho) \frac{\cos(p\varphi)}{\sqrt{\pi}} + b_p^{Ys} Y_p(k\rho) \frac{\sin(p\varphi)}{\sqrt{\pi}} + b_p^{Yc} Y_p(k\rho) \frac{\cos(p\varphi)}{\sqrt{\pi}} \right\}. \quad (11)$$

Amplitudes are again arranged in vectors:

$$\vec{b}^J = \begin{bmatrix} b_0^J \\ b_1^{Js} \\ b_2^{Js} \\ \vdots \\ b_1^{Jc} \\ b_2^{Jc} \\ \vdots \end{bmatrix} \qquad \vec{b}^Y = \begin{bmatrix} b_0^Y \\ b_1^{Ys} \\ b_2^{Ys} \\ \vdots \\ b_1^{Yc} \\ b_2^{Yc} \\ \vdots \end{bmatrix}. \tag{12}$$

The coordinate transformation in [25] yields relations between the amplitude vectors (6) and (12):

$$\vec{b}^J = \boldsymbol{G}^J \cdot \vec{a}^J \qquad \vec{b}^Y = \boldsymbol{G}^J \cdot \vec{a}^Y \tag{13}$$

$$\boldsymbol{G}^J = \begin{bmatrix} g^{J00} & g_1^{J0s} & g_2^{J0s} & \cdots & g_1^{J0c} & g_2^{J0c} & \cdots \\ g_1^{Js0} & g_{11}^{Jss} & g_{12}^{Jss} & \cdots & g_{11}^{Jsc} & g_{12}^{Jsc} & \cdots \\ g_2^{Js0} & g_{21}^{Jss} & g_{22}^{Jss} & \cdots & g_{21}^{Jsc} & g_{22}^{Jsc} & \cdots \\ \vdots & \vdots & \vdots & \ddots & \vdots & \vdots & \ddots \\ g_1^{Jc0} & g_{11}^{Jcs} & g_{12}^{Jcs} & \cdots & g_{11}^{Jcc} & g_{12}^{Jcc} & \cdots \\ g_2^{Jc0} & g_{21}^{Jcs} & g_{22}^{Jcs} & \cdots & g_{21}^{Jcc} & g_{22}^{Jcc} & \cdots \\ \vdots & \vdots & \vdots & \ddots & \vdots & \vdots & \ddots \end{bmatrix} \tag{14}$$

$$g^{J00} = J_0(kd)$$

$$g_n^{J0s} = (-1)^n \sqrt{2}\, J_n(kd) \sin\frac{n\pi}{2}$$

$$g_n^{J0c} = (-1)^n \sqrt{2}\, J_n(kd) \cos\frac{n\pi}{2}$$

$$g_p^{Js0} = \sqrt{2}\, J_p(kd) \sin\frac{n\pi}{2}$$

$$g_p^{Jc0} = \sqrt{2}\, J_p(kd) \cos\frac{n\pi}{2}$$

To perform the orthogonal expansion method, it is suitable to condense the ρ-dependent terms of (11) to new functions $U_0(k\rho)$, $U_p^s(k\rho)$, and $U_p^c(k\rho)$:

$$A_z = U_0(k\rho)\frac{1}{\sqrt{2\pi}} + \sum_{p=1}^{\infty}\left\{ U_p^s(k\rho)\frac{\sin(p\varphi)}{\sqrt{\pi}} + U_p^c(k\rho)\frac{\cos(p\varphi)}{\sqrt{\pi}} \right\}. \tag{16}$$

A_z is proportional to the tangential electric field component on the interaction region surface E_z. To consider the tangential magnetic field component H_φ, the following function is defined introducing $I_0(k\rho)$, $I_p^s(k\rho)$, and $I_p^c(k\rho)$:

$$H_\varphi h = -\frac{\partial A_z}{\partial \rho} h = I_0(k\rho)\frac{1}{\sqrt{2\pi}} + \sum_{p=1}^{\infty}\left\{ I_p^s(k\rho)\frac{\sin(p\varphi)}{\sqrt{\pi}} + I_p^c(k\rho)\frac{\cos(p\varphi)}{\sqrt{\pi}} \right\}. \tag{17}$$

The new functions from (16) and (17) are arranged in vectors:

$$\vec{U}(k\rho) = \begin{bmatrix} U_0(k\rho) \\ U_1^s(k\rho) \\ U_2^s(k\rho) \\ \vdots \\ U_1^c(k\rho) \\ U_2^c(k\rho) \\ \vdots \end{bmatrix} \qquad \vec{I}(k\rho) = \begin{bmatrix} I_0(k\rho) \\ I_1^s(k\rho) \\ I_2^s(k\rho) \\ \vdots \\ I_1^c(k\rho) \\ I_2^c(k\rho) \\ \vdots \end{bmatrix}. \tag{18}$$

$$g_{pn}^{Jss} = J_{p-n}(kd)\cos\frac{(p-n)\pi}{2} - (-1)^n J_{p+n}(kd)\cos\frac{(p+n)\pi}{2}$$

$$g_{pn}^{Jsc} = J_{p-n}(kd)\sin\frac{(p-n)\pi}{2} + (-1)^n J_{p+n}(kd)\sin\frac{(p+n)\pi}{2}$$

$$g_{pn}^{Jcs} = -J_{p-n}(kd)\sin\frac{(p-n)\pi}{2} + (-1)^n J_{p+n}(kd)\sin\frac{(p+n)\pi}{2}$$

$$g_{pn}^{Jcc} = J_{p-n}(kd)\cos\frac{(p-n)\pi}{2} + (-1)^n J_{p+n}(kd)\cos\frac{(p+n)\pi}{2}$$

$$d = b - \frac{h}{2}. \tag{15}$$

The Bessel functions from (11) are arranged in matrices:

$$\boldsymbol{J}(k\rho)=\begin{bmatrix} J_0(k\rho) & & & & & & \\ & J_1(k\rho) & & 0 & & & \\ & & J_2(k\rho) & & & & \\ & & & \ddots & & & \\ & & & & J_1(k\rho) & & \\ & 0 & & & & J_2(k\rho) & \\ & & & & & & \ddots \end{bmatrix}$$

$$\boldsymbol{Y}(k\rho)=\begin{bmatrix} Y_0(k\rho) & & & & & & \\ & Y_1(k\rho) & & 0 & & & \\ & & Y_2(k\rho) & & & & \\ & & & \ddots & & & \\ & & & & Y_1(k\rho) & & \\ & 0 & & & & Y_2(k\rho) & \\ & & & & & & \ddots \end{bmatrix}. \tag{19}$$

By means of (11), the vectors (18) of (16) and (17) read

$$\vec{U}(k\rho)=\boldsymbol{J}(k\rho)\cdot\vec{b}^{J}+\boldsymbol{Y}(k\rho)\cdot\vec{b}^{Y} \tag{20}$$

$$\vec{I}(k\rho)=-hk\left\{\boldsymbol{J}'(k\rho)\cdot\vec{b}^{J}+\boldsymbol{Y}'(k\rho)\cdot\vec{b}^{Y}\right\}. \tag{21}$$

The vectors $\vec{b}^{J}$ and $\vec{b}^{Y}$ are replaced using the transformation (13). Then $\vec{a}^{Y}$ is replaced using (7). Finally, $\vec{a}^{J}$ is eliminated. A relation between $\vec{U}(k\rho)$ and $\vec{I}(k\rho)$ follows, which can be written by the matrix $\boldsymbol{Z}(k\rho)$:

$$\vec{U}(k\rho)=\boldsymbol{Z}(k\rho)\cdot\vec{I}(k\rho) \tag{22}$$

$$\boldsymbol{Z}(k\rho)=\frac{-1}{hk}\left\{\boldsymbol{J}(k\rho)\cdot\boldsymbol{G}^{J}+\boldsymbol{Y}(k\rho)\cdot\boldsymbol{G}^{J}\cdot\boldsymbol{\xi}\right\}\cdot\left\{\boldsymbol{J}'(k\rho)\cdot\boldsymbol{G}^{J}+\boldsymbol{Y}'(k\rho)\cdot\boldsymbol{G}^{J}\cdot\boldsymbol{\xi}\right\}^{-1}. \tag{23}$$

For the following development of the continuity conditions on the surface of the interaction region ($\rho=R$) by the orthogonal expansion method, the field formulations (16) and (17) are used. The continuity conditions on the surface of the dielectric cylinder are considered by the matrix $\boldsymbol{Z}(k\rho)$ from (22).

B. Scattering Parameters

In the waveguide regions W1 and W2, all TE_{m0} modes are to be considered. In the Cartesian coordinate system x, y, z of Fig. 2, these are modes with the field components H_x, H_y, and E_z which are propagating in the $\pm x$ direction.

Waveguide region W1 ($-\infty < x < 0$):

$$A_z=\sum_{m=1}^{\infty}\sin\frac{m\pi y}{h}\left\{q_m e^{-j k_{xm}x}+r_m e^{+j k_{xm}x}\right\}. \tag{24}$$

Waveguide region W2 ($0 < x < \infty$):

$$A_z=\sum_{m=1}^{\infty}\sin\frac{m\pi y}{h}\left\{t_m e^{-j k_{xm}x}+s_m e^{+j k_{xm}x}\right\} \tag{25}$$

$$k_{xm}=\sqrt{\omega^2\epsilon_0\mu_0-\left(\frac{m\pi}{h}\right)^2}. \tag{26}$$

For a correct field matching in the whole interaction region, the fields (24) and (25) must be defined for $x<0$ and $x>0$, respectively. For $x<-r$ and $x>r$, the validity of (24) and (25) is obvious. In the region $-r\leqslant x\leqslant r$ the fields of the interaction region of (16) and (17) can be continued analytically. Only at $x=0$, a pole will occur because of the Y functions. Therefore it is sufficient to exclude only the plane $x=0$ from the definition regions of (24) and (25). A former discussion about the validity of field representtions for a related problem is given by Lewin [26], [27]. In [6] and [7], the same regions as in our method are used.

The eigenfunctions of the waveguide fields are abbreviated as follows:

$$\Phi_m^{q}(x,y)=\Phi_m^{t}(x,y)=\sin\frac{m\pi y}{h}e^{-j k_{xm}x} \tag{27}$$

$$\Phi_m^{r}(x,y)=\Phi_m^{s}(x,y)=\sin\frac{m\pi y}{h}e^{+j k_{xm}x}. \tag{28}$$

The transformation to the cylindrical coordinates of the interaction region yields

$$\Phi_m^{q}(\rho,\varphi)=\Phi_m^{t}(\rho,\varphi)=\sin\frac{m\pi(b+\rho\sin\varphi)}{h}e^{-j k_{xm}\rho\cos\varphi}$$

$$\Phi_m^{r}(\rho,\varphi)=\Phi_m^{s}(\rho,\varphi)=\sin\frac{m\pi(b+\rho\sin\varphi)}{h}e^{+j k_{xm}\rho\cos\varphi}. \tag{29}$$

The ρ derivatives are also abbreviated:

$$\Psi_m^q(\rho,\varphi) = -\frac{\partial \Phi_m^q(\rho,\varphi)}{\partial \rho} h$$

$$\Psi_m^t(\rho,\varphi) = -\frac{\partial \Phi_m^t(\rho,\varphi)}{\partial \rho} h$$

$$\Psi_m^r(\rho,\varphi) = -\frac{\partial \Phi_m^r(\rho,\varphi)}{\partial \rho} h$$

$$\Psi_m^s(\rho,\varphi) = -\frac{\partial \Phi_m^s(\rho,\varphi)}{\partial \rho} h. \tag{30}$$

The orthonormal eigenfunctions dependent on φ from (16) and (17) are arranged in a vector:

$$\vec{T}(\varphi) = \begin{bmatrix} 1/\sqrt{2} \\ \sin\varphi \\ \sin 2\varphi \\ \vdots \\ \cos\varphi \\ \cos 2\varphi \\ \vdots \end{bmatrix}. \tag{31}$$

To obtain the continuity conditions on the surface of the interaction region, (16) and (17) are multiplied with the elements of $\vec{T}$. Integration by φ in the range of $-\pi/2$ to $3\pi/2$ yields [17], [20], [23]

Continuity of E_z:

$$\vec{U}(kR) = \sum_{m=1}^{\infty} \left\{ q_m \int_{\pi/2}^{3/2\pi} \vec{T}(\varphi)\Phi_m^q(R,\varphi)\,d\varphi + s_m \int_{\pi/2}^{\pi/2} \vec{T}(\varphi)\Phi_m^s(R,\varphi)\,d\varphi + r_m \int_{\pi/2}^{3/2\pi} \vec{T}(\varphi)\Phi_m^r(R,\varphi)\,d\varphi + t_m \int_{\pi/2}^{\pi/2} \vec{T}(\varphi)\Phi_m^t(R,\varphi)\,d\varphi \right\}. \tag{32}$$

Continuity of H_φ:

$$\vec{I}(kR) = \sum_{m=1}^{\infty} \left\{ q_m \int_{\pi/2}^{3/2\pi} \vec{T}(\varphi)\Psi_m^q(R,\varphi)\,d\varphi + s_m \int_{\pi/2}^{\pi/2} \vec{T}(\varphi)\Psi_m^s(R,\varphi)\,d\varphi + r_m \int_{\pi/2}^{3/2\pi} \vec{T}(\varphi)\Psi_m^r(R,\varphi)\,d\varphi + t_m \int_{\pi/2}^{\pi/2} \vec{T}(\varphi)\Psi_m^t(R,\varphi)\,d\varphi \right\}. \tag{33}$$

To obtain the integrals from (32), the integrands are expanded to Bessel functions [28], [29]:

$$\vec{T}(\varphi)\sin\frac{m\pi(b+\rho\cdot\sin\varphi)}{h} e^{\mp jk_{xm}\rho\cos\varphi} = \sum_{i=-\infty}^{i=\infty} \vec{T}(\varphi)\sin\left(i\varphi + \frac{m\pi b}{h}\right) J_i\left(\sqrt{(hk_{xm})^2+(m\pi)^2}\,\frac{\rho}{h}\right) \cdot \begin{cases} e^{\mp ji\arctan\frac{hk_{xm}}{m\pi}}, & k_{xm}^2 \geq 0 \\ \left[\dfrac{m\pi \pm \sqrt{-k_{xm}^2}}{m\pi \mp \sqrt{-k_{xm}^2}}\right]^{1/2}, & k_{xm}^2 < 0. \end{cases} \tag{34}$$

After exchanging integration and summation, the φ-dependent terms can be integrated analytically. Derivation with respect to ρ yields the terms of the sums which are used to calculate the integrals from (13). Now the integrals are arranged in matrices:

$$\vec{U}(kR) = \boldsymbol{K}^{UE}\cdot\begin{bmatrix} q_1 \\ q_2 \\ \vdots \\ s_1 \\ s_2 \\ \vdots \end{bmatrix} + \boldsymbol{K}^{UA}\cdot\begin{bmatrix} r_1 \\ r_2 \\ \vdots \\ t_1 \\ t_2 \\ \vdots \end{bmatrix} \tag{35}$$

$$\vec{I}(kR) = \boldsymbol{K}^{IE}\cdot\begin{bmatrix} q_1 \\ q_2 \\ \vdots \\ s_1 \\ s_2 \\ \vdots \end{bmatrix} + \boldsymbol{K}^{IA}\cdot\begin{bmatrix} r_1 \\ r_2 \\ \vdots \\ t_1 \\ t_2 \\ \vdots \end{bmatrix}. \tag{36}$$

Taking into account (22), the scattering matrix can be obtained by (35) and (36):

$$\begin{bmatrix} r_1 \\ r_2 \\ \vdots \\ t_1 \\ t_2 \\ \vdots \end{bmatrix} = \boldsymbol{S}\cdot\begin{bmatrix} q_1 \\ q_2 \\ \vdots \\ s_1 \\ s_2 \\ \vdots \end{bmatrix} \tag{37}$$

$$\boldsymbol{S} = \left\{\boldsymbol{K}^{UA} - \boldsymbol{Z}(kR)\cdot\boldsymbol{K}^{IA}\right\}^{-1}\cdot\left\{\boldsymbol{Z}(kR)\cdot\boldsymbol{K}^{IE} - \boldsymbol{K}^{UE}\right\}. \tag{38}$$

C. Numerical Investigation

For numerical investigation, the infinite sums of the exact mathematical formulation must be approximated by finite sums. An examination of the scattering parameters and field convergence yields criteria for the truncation of the sums. For an accuracy of the TE_{10}-mode scattering coefficients (t_1 and r_1) better than 1 percent and not too

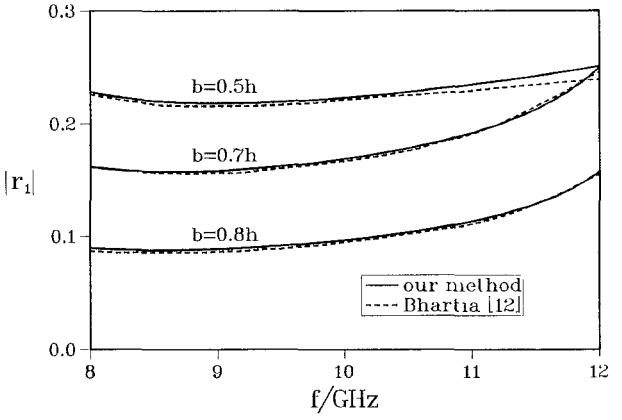

Fig. 3. Comparison with Bhartia [12]. $\epsilon_r = 4.4$; $\tan\delta = 2.955\times10^{-2}$; $r = 0.05625h$; $b = 0.5h, 0.6h, 0.7h$.

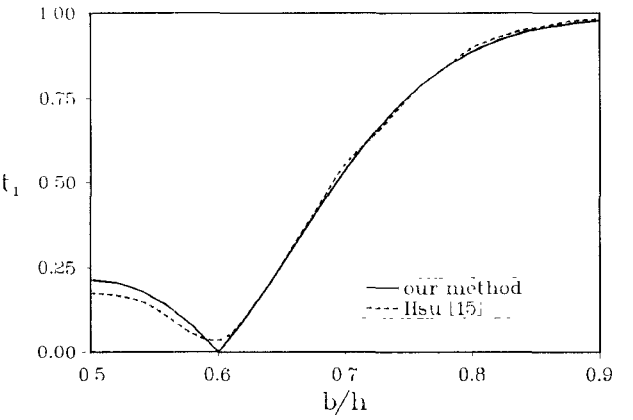

Fig. 4. Comparison with Hsu [15]. $f = 9.37$ GHz; $\epsilon_r = 38$; $\tan\delta = 0$; $r = 0.075h$.

large post radius and permittivity ($\epsilon_r r/h < 10$), the following numbers of eigenfunctions have to be considered:

interaction region: IR: $n_{max} = p_{max} = 10$

waveguide regions: W1: $m_{max} = 10$ W2: $m_{max} = 11$. (39)

The numbers of eigenfunctions in both waveguide regions have to be different in order to obtain quadratic matrices in (38). Their sum has to be equal to the number of eigenfunctions in IR, $2p_{max}+1$. With the wavenumbers from (39), the computation of one scattering matrix needs about 3.5 s on an IBM 4381 computer.

For accurate field patterns, higher order scattering coefficients must be precisely computed, so more eigenfunctions have to be considered:

interaction region: IR: $n_{max} = p_{max} = 25$

waveguide regions: W1: $m_{max} = 25$ W2: $m_{max} = 26$. (40)

III. Results

Numerical results are given for a R-100 waveguide with the following width:

$$h = 22.86 \text{ mm} = 9/10 \text{ in.} \quad (41)$$

The cutoff frequency of the TE_{10} mode is 6.56 GHz; frequency respsonses are given in the technically used range 8 GHz–12 GHz. All dimensions are normalized with respect to the waveguide width h.

A. Comparison with Other Authors

Scattering parameters are compared with results from [12] (Fig. 3) and [15] (Fig. 4). The reflection coefficients $|r_1|$ of a lossy dielectric rod calculated by Bhartia [12] agree with our results within drawing precision except for the symmetric case ($b = 0.5h$) near 12 GHz. Hsu and Auda [15] show the transmission coefficient $|t_1|$ as a function of the post position b/h. Below the minimum of $|t_1|$ at $b = 0.6h$, there is a small discrepancy between the curves which disappears above $b = 0.6h$.

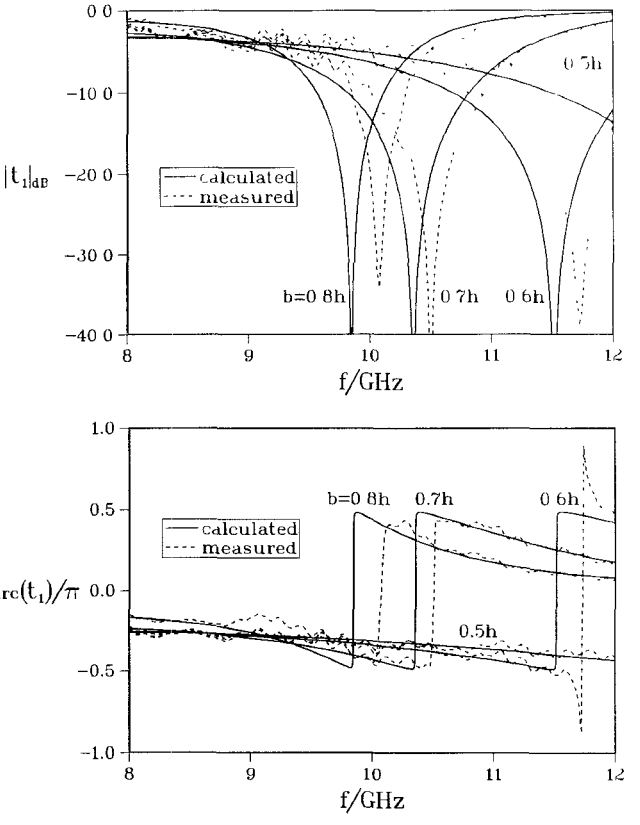

Fig. 5 Frequency responses of a bandstop filter. $\epsilon_r = 38.5$; $\tan\delta = 2\times10^{-4}$; $r = 0.03h$; $b = 0.5h, 0.6h, 0.7h, 0.8h$.

B. Bandstop Filter

To design bandstop filtes with suitable characteristics, a dieletric material is chosen with a high permittivity ($\epsilon_r = 38.5$), low losses ($\tan\delta = 2\times10^{-4}$), and an eligible temperature coefficient as described by Pöbl and Wolfram [30].

Figs. 5 and 6 show the calculated and measured frequency responses of the transmission coefficient t_1 for several post positions b. Though a small cylinder radius is chosen ($r = 0.03$h), stopbands occur with a theoretical attentuation greater than 40 dB. The measured attenuation decreases from about 40 dB ($0.6h \leqslant b \leqslant 0.7h$) to 15 dB ($b = 0.925h$). Moving the post from the waveguide center to one side wall, the resonance frequency decreases (Fig. 5,

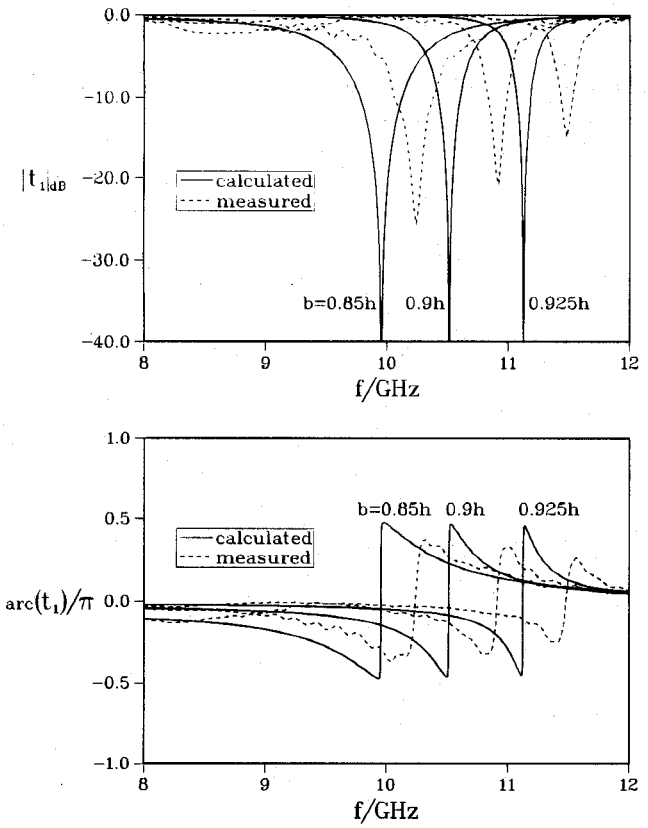

Fig. 6. Frequency responses of a bandstop filter. $\epsilon_r = 38.5$; $\tan\delta = 2\times 10^{-4}$; $r = 0.03h$; $b = 0.85h, 0.9h, 0.925h$.

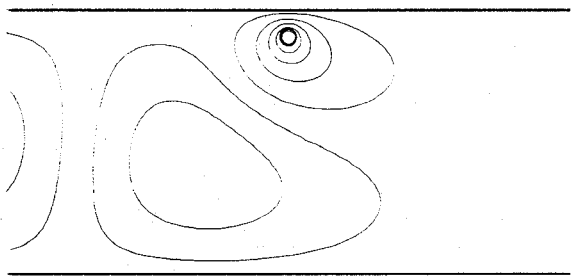

Fig. 7. Magnetic field in a bandstop filter at resonance frequency. $f = 10.52$ GHz; $\omega t = 0.5\pi$; $|t_1| = -50$ dB; $\epsilon_r = 38.5$; $\tan\delta = 2\times 10^{-4}$; $r = 0.03h$; $b = 0.9h$.

$0.5h \leqslant b \leqslant 0.8h$) and increases again (Fig. 6, $0.85h \leqslant b \leqslant 0.925h$). At the same time, the bandwidth decreases. So a certain resonance frequency in the range from 10 GHz to 12 GHz can be achieved by two alternative post positions, thereby obtaining different bandwidths.

The principal calculated effects are proved by measurement. Divergences occur mainly at resonance effects. The measured attenuation is smaller than the calculated value because of waveguide and measurement device losses, which are not considered in the analysis. (The equipment used was not optimized to obtain low losses.) Furthermore, measured resonance frequencies are higher than calculated ones. Possible reasons are tolerances of the dielectric constant and cylinder radius, which have a great influence on resonance frequencies.

Magnetic fields at resonance are shown in Fig. 7. Because of the low transmission coefficient ($|t_1| = -50$ dB),

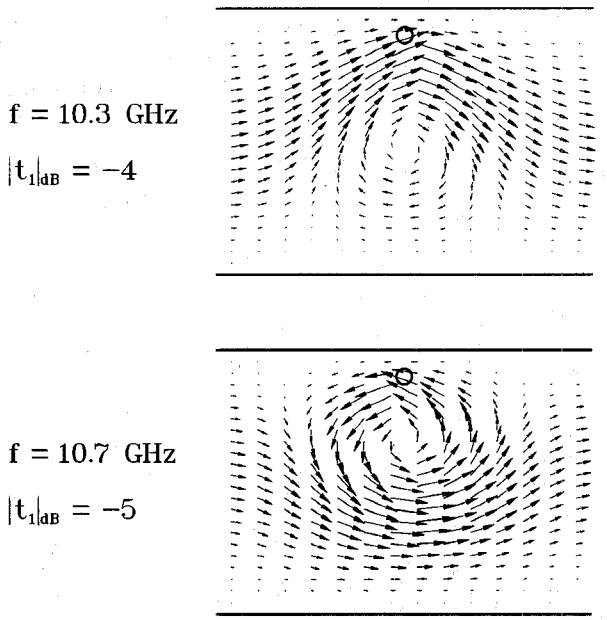

Fig. 8. Poynting vector in a bandstop filter below and above resonance frequency. $\epsilon_r = 38.5$; $\tan\delta = 2\times 10^{-4}$; $r = 0.03h$; $b = 0.9h$.

there is no wave propagation in the waveguide region W2. In W1, a standing wave occurs. Inside and near the post, a concentric magnetic field occurs. The location of field extrema is time-independent. At the chosen time ($\omega t = 0.5\pi$), the field strengths are maximal; at $\omega t = 0$, all fields vanish. Resonance occurs as an interaction between the fields of the dielectric cylinder and the waveguide walls. In the region of the post, fields are similar to those of the TE_{20} mode of the empty waveguide. The resonance can be explained by the occurrence of TE_{20}-type fields at cutoff frequency in a dielectric loaded waveguide region. Note that the resonance fields are asymmetric to the waveguide and therefore cannot be obtained by the discussion of a centered post.

Poynting vectors below and above resonance frequency are shown in Fig. 8. In both diagrams, a vortex of power flow occurs. Below resonance, the power is transported through the rod in the propagation direction of the waveguide. At resonance, the rotation direction of the vortex changes and the transmission becomes minimal. Above resonance, the power is transported through the waveguide in the lower region ($0 < y < 0.5h$). The physical mechanism of power flow changes at resonance. Below resonance, the power distribution is caused by the TE_{10} mode. Above resonance, the occurring TE_{20} mode changes the power distribution.

IV. Conclusions

A method is presented which obtains accurate results and field patterns for a lossy dielectric cylinder in a rectangular waveguide. The lowest resonance mode in the fundamental-mode frequency range is used to realize a tunable bandstop filter. As shown by the field patterns, the resonance is caused by an interaction between the dielectric cylinder and the waveguide walls. For this resonance

mode, posts are smaller than those used today in technical applications.

To design higher order filters, post can be located in series by simple scattering-matrix operations. For an effective design of multiple-post structures, knowledge of the principal physical effects of the one-post structure shown here is useful becaus of the variety of effects and possible structures.

ACKNOWLEDGMENT

The authors would like to thank Prof. Dr.-Ing. G. Piefke and the members of his staff for helpful discussions.

REFERENCES

[1] N. Marcuvitz, *Waveguide Handbook*. New York: McGraw-Hill, 1951.
[2] K. W. H. Foulds, "Simple calculation of the equivalent circuit of loss-free obstacles," *Proc. IEEE*, vol. 12, pp. 2180–2186, 1965.
[3] L. Lewin, *Theory of Waveguides*. London: Butterworth, 1975.
[4] E. D. Nielsen, "Scattering by a cylindrical post of complex permittivity in a waveguide," *IEEE Trans. Microwave Theory Tech.*, vol. MTT-17, pp. 148–153, 1969.
[5] J. B. Andersen and B. Majborn, "Semiconductor rod in waveguide —Field distribution for positive and negative conductivity," *IEEE Trans. Microwave Theory Tech.*, vol. MTT-16, pp. 194–196, 1968.
[6] N. Gotsis, E. E. Vafiadis, and J. N. Sahalos, "The discontinuity problem of a cylindrical dielectric post in a waveguide and its application on the dielectric constant measurements of liquids," *Arch. Elektrotech.*, vol. 68, pp. 249–257, 1985.
[7] J. N. Sahalos and E. Vafiadis, "On the narrow-band microwave filter design using a dielectric rod," *IEEE Trans. Microwave Theory Tech.*, vol. MTT-33, pp. 1165–1171, 1985.
[8] N. Okamoto, J. Nishioka, and Y. Nakanishi, "Scattering by a ferrimagnetic circular cylinder in a rectangular waveguide," *IEEE Trans. Microwave Theory Tech.*, vol. MTT-19, pp. 521–527, 1971.
[9] N. Okamoto and Y. Nakanishi, "Correction to 'Scattering by a ferrimagnetic cylinder in a rectangular waveguide,'" *IEEE Trans. Microwave Theory Tech.*, vol. MTT-20, pp. 782–783, 1972.
[10] P. Bhartia, "Comments on 'Scattering by a ferrimagnetic cylinder in a rectangular waveguide,'" *IEEE Trans. Microwave Theory Tech.*, vol. MTT-22, p. 975, 1974.
[11] T. Yoshida, M. Umeno, and S. Miki, "Propagation characteristics of a rectangular waveguide containing a cylindrical rod of magnetized ferrite," *IEEE Trans. Microwave Theory Tech.*, vol. MTT-20, pp. 739–743, 1972.
[12] P. Bhartia, "Dielectric rod loaded waveguides," *Arch. Elek. Übertragung.*, vol. 31, pp. 60–62, 1977.
[13] G. Cicconi and C. Rosatelli, "Solutions of the vector wave equation for inhomogeneous dielectric cylinders—Scattering in waveguides," *IEEE Trans. Microwave Theory Tech.*, vol. MTT-25, pp. 885–892, 1977.
[14] J. C. Araneta, M. E. Brodwin, and G. A. Kriegsmann, "High-temperature characterisation of dielectric rods," *IEEE Trans. Microwave Theory Tech.*, vol. MTT-32, pp. 1328–1335, 1984.
[15] C. G. Hsu and H. A. Auda, "Multiple dielectric posts in a rectangular waveguide," *IEEE Trans. Microwave Theory Tech.*, vol. MTT-34, pp. 883–891, 1986.
[16] Y. Leviatan and G. S. Sheaffer, "Analysis of inductive dielectric posts in rectangular waveguide," *IEEE Trans. Microwave Theory Tech.*, vol. MTT-35, pp. 48–59, 1987.
[17] J. Lauterjung, *Abstrahlungs- und Beugungsprobleme in Hohlleiterstrukturen mit mit isotropen und magnetisch gyrotropen kreiszylindrischen Streukörpern*, Darmstädter Dissertation D17, Darmstadt, 1982.
[18] N. Löchel, *Untersuchung eines Rechteckhohlleiters mit außermittig angebrachtem, dielektrischen Stift*, Diplomarbeit am Fachgebiet Theoretische Elektrotechnik der Technischen Hochschule Darmstadt, Darmstadt, 1984.
[19] R. Gesche, "Resonanzeffekte eines kreiszylindrischen, dielektrischen Streukörpers im Rechteckhohlleiter," *Kleinheubacher Berichte*, vol. 28, pp. 223–228, 1985.
[20] R. Gesche, *Kreiszylindrische Streukörper im Rechteckhohlleiter*, Darmstädter Dissertation D17, Darmstadt, 1986.
[21] G. Piefke, "Das dreidimensionale Zwischenmedium in der Feldtheorie," *Arch. Elek. Übertragung.*, vol. 24, p. 523, 1970.
[22] G. Piefke, *Feldtheorie III*, Bibl. Inst., Mannheim, 1977.
[23] F. Reisdorf, *Die Zwischenmediums-Methode*, Darmstädter Dissertation D17, Darmstadt, 1977.
[24] G. Piefke, *Feldtheorie I*, Bibl. Inst., Mannheim, 1977.
[25] R. Gesche, "Transformation of the wave equation solution between parallen displaced cylindrical coordinate systems," *Arch. Elektrotech.*, vol. 67, pp. 391–394, 1984.
[26] L. Lewin, "On the inadequacy of discrete mode-matching techniques in some waveguide discontinuity problems," *IEEE Trans. Microwave Theory Tech.*, vol. MTT-18, pp. 364–372, 1970.
[27] L. Lewin, "On the restricted validity of point-matching techniques," *IEEE Trans. Microwave Theory Tech.*, vol. MTT-18, pp. 1041–1047, 1970.
[28] F. Reisdorf and H. Knetsch, "Wellenausbreitung im abgeknickten Rechteckhohlleiter," *Nachrichtentech. Z.*, pp. 312–317, 1972.
[29] S. Russenschuck, *Berechnung der Koppelintegrale zwischen den Eigenwellen im Rechteckhohlleiter und den Lösungen der Wellengleichung in Zylinderkoordinaten*, Studienarbeit am Fachgebeiet Theoretische Elektrotechnik der Technischen Hochschule Darmstadt, Darmstadt, 1985.
[30] K. Pöbl and G. Wolfram, "Dielektrische Resonatoren, neue Bauelemente der Mikrowellentechnik," *Siemens Components*, vol. 20, pp. 14–18, 1982.

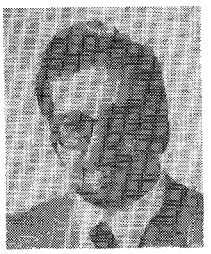

Roland Gesche (M'87) was born in Berlin, Germany, on June 18, 1957. He received the Diplom-Ingenieur and the Doktor-Ingenieur degrees from the Technical University of Darmstadt, Germany, in 1982 and 1986. From 1981 to 1982 he was employed as a research assistant at the Technical University of Darmstadt. Since 1987 he has been engaged in the investigation of RF equipment at Leybold AG, Alzenau.

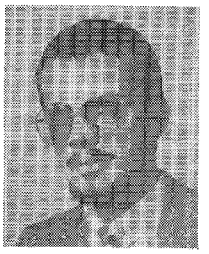

Norbert Löchel was born in Marburg, Germany, on August 1, 1958. After receiving the Diplom-Ingenieur degree from the Technical University of Darmstadt, he joined the Siemens AG, München, where he is engaged in the development of microwave systems.